Soret-Excited Raman Spectroscopy of the Spinach Cytochrome b_6f Complex. Structures of the *b*- and *c*-Type Hemes, Chlorophyll *a*, and β-Carotene

Thierry Picaud, Carole Le Moigne, Adrienne Gomez de Gracia, and Alain Desbois*

Département de Biologie Cellulaire et Moléculaire, Section de Biophysique des Protéines et des Membranes, CEA et CNRS URA 2096, CEA/Saclay, F-91191 Gif-sur-Yvette Cedex, France

Received August 8, 2000

ABSTRACT: Soret-excited resonance Raman (RR) spectra of the spinach cytochrome b_6f complex (cyt b_6f) are reported for the oxidized, native, ascorbate-reduced, and dithionite-reduced forms. Using excitations at 441.6, 413.1, and 406.7 nm, RR contributions of chlorophyll *a*, β-carotene, the *c*-type heme of cytochrome *f*, and the *b*-type hemes of cytochrome b_6 of the b_6f complex were identified and the data compared to those previously obtained for the *Rhodospirillum rubrum* bc_1 complex [Le Moigne, C., Schoepp, B., Othman, S., Verméglio, A., and Desbois, A. (1999) *Biochemistry 38*, 1066−1076]. RR bands arising from the b_6f-associated chlorophyll *a* and β-carotene pigments were found to be particularly intense in the spectra excited at 441.6 nm. The frequencies of the phorbin skeleton of chlorophyll *a* at 1606, 1552, and 1525 cm^{-1} are typical of a Mg atom with a single axial ligand. Strong RR bands corresponding to stretching or deformation modes of β-carotene were detected at 1137, 1157, 1191, 1216, and 1531 cm^{-1} in the different forms of cyt b_6f. This set of frequencies is assigned to an *all-trans* configuration of the polyene chain. The redox titrations of the b_6f complex allow the characterization of RR bands of the three hemes. The ν_{10}, ν_2, ν_3, and ν_8 modes of reduced cyt *f* are detected at 1619, 1591, 1492, and 356 cm^{-1}, respectively. From this set of frequencies, one can conclude that the particular histidine/amine heme coordination found in the truncated soluble domain of cyt *f* is a specific feature of the entire cyt *f* included in the b_6f complex. The frequencies of the ν_2, ν_8, and ν_{10} marker modes are consistent with different conformations for the two *b*-type hemes of cyt b_6f. One of these hemes is strongly distorted (ν_2, ν_8, and ν_{10} at 1581, 351, and 1610 cm^{-1}, respectively), while the other one is planar (1586, 345, and 1618 cm^{-1}, respectively). Largely different structures for the *b*-type hemes appear to be a common property for the bc_1/b_6f complexes.

The cytochrome b_6f complex (plastoquinol:plastocyanin oxidoreductase, EC 1.10.99.1) (cyt b_6f)[1] is an integral membrane protein involved in electron transfer and proton translocation in chloroplast thylakoids and cyanobacteria (*1*−*3*). It exhibits overall functional similarities with the evolutionarily related cytochrome bc_1 complex (ubiquinol:cytochrome c_1 oxidoreductase) (cyt bc_1) of mitochondria and photosynthetic bacteria (*4*, *5*). Cyt b_6f participates in the oxygenic photosynthesis as a redox link between the two reaction center complexes, accepts electrons from a quinone carrier (designated as plastoquinol), and translocates protons across the membrane, generating an energy source for ATP synthesis. Cytochrome bc_1/b_6f complexes show a similar membrane topology in the arrangement of the subunits containing the redox prosthetic groups, i.e., cytochrome b_6 (cyt b_6) with two *b*-type hemes, cytochrome *f* (cyt *f*) with a *c*-type heme, and the Rieske protein with a [2Fe-2S] center (*6*−*9*). The purified cyt b_6f complexes are generally dimeric (*10*, *11*). Each monomer contains a core of four protein subunits, i.e., the cyt b_6 subunit (M_w = 24 kDa), cyt *f* (M_w = 32 kDa), the Rieske protein (M_w = 19 kDa), and subunit IV (M_w = 17.5 kDa). In higher plants and green algae, three small additional polypeptides ($M_w \sim 4$ kDa) copurify with the four preceding subunits (*12*, *13*). Sequence comparisons showed that cyt b_6 represents the half N-terminal heme-binding domain of mitochondrial and bacterial cyt *b* (*6*). Subunit IV has no prosthetic group but is homologous to the C-terminal part of cyt *b* (*6*). Like cyt *b*, the cyt b_6 subunit contains a low- and a high-potential *b*-type heme (heme b_L and heme b_H, respectively). At pH 7.4, the midpoint potentials of heme b_L and b_H are −170 (±20) and −70 (±25) mV, respectively (*13*, *14*). In the crystal structure of bovine cyt bc_1, the axial ligands of heme b_L are His-83 and His-182 while those of heme b_H are His-97 and His-196 (*7*). These four His residues are absolutely invariant in the sequences of cyt *b* and cyt b_6 (*6*, *15*, *16*). The differences in the visible absorption spectra of hemes b_H and b_L are less marked for cyt b_6f than for cyt bc_1 (*17*, *18*). The EPR spectra, however, show a strained coordination for the two *b*-type hemes of the bc_1 and b_6f complexes (*19*, *20*). Cyt *f* carries a covalently bound *c*-type heme. Its redox potential is comprised between +290 and +370 mV (*13*, *21*−*23*). The [2Fe-2S] cluster of the Rieske protein has in average a slightly lower potential than that of cyt *f* (+290−320 mV) (*21*, *24*, *25*).

* To whom correspondence should be addressed. Fax: 33 (0)1.69.08.43.89. E-mail: desbois@dsvidf.cea.fr.

[1] Abbreviations: RR, resonance Raman; cyt, cytochrome; cyt b_6f, cytochrome b_6f complex; cyt bc_1, cytochrome bc_1 complex; Chl_a, chlorophyll *a*; β-Car, β-carotene; MEGA-9, nonanoyl-*N*-methylglucamide.

10.1021/bi0106641 CCC: $20.00
Published on Web 05/24/2001

The dimeric b_6f complexes isolated from different species bind chlorophyll *a* (Chl$_a$) with a Chl$_a$/cyt *f* ratio of 0.8−1.7 (*10*, *11*, *26*−*28*). β-Carotene (β-Car) also binds to cyt b_6f with a stoichiometry relative to cyt *f* varying from 0.3 to 1.0 (*11*, *28*). The binding sites of Chl$_a$ and β-Car were not precisely identified. However, Chl$_a$ was located in the cyt b_6 polypeptide and β-Car close to Chl$_a$ (*28*, *29*).

No tridimensional information is available for a b_6f complex while several structures were solved for mitochondrial bc_1 complexes (*7*, *9*, *30*). Atomic structures were, however, determined for soluble domains of Rieske proteins and of cyt *f* (*31*−*35*). On one hand, the data show that the Rieske proteins of the bc_1/b_6f complexes have diverged despite a common fold. Nevertheless, the [2Fe-2S] cluster-binding subdomains are identical (*32*, *33*). On the other hand, the *c*-type cytochromes of the bc_1/b_6f complexes are unrelated proteins with different heme ligation and polypeptide folding (*30*, *31*, *34*, *35*). A common architecture for the bc_1/b_6f transmembrane core is apparent in the conserved sequences of cyt *b* for the bc_1 complexes and of cyt b_6 and subunit IV for the b_6f complexes (*6*). Despite this conservation, it is not quite certain that the structures of hemes b_H and b_L are identical in the bc_1 and b_6f complexes. In particular, the different subunit composition and pigment content in the complexes could influence the structure of the *b*-type hemes. We have recently used resonance Raman (RR) spectroscopy in characterizing the heme sites of the bc_1 complex purified from *Rhodospirillum rubrum* (*36*). In this work, we have employed this vibrational spectroscopy to gain more insight into the molecular structure of the hemes, which is a prerequisite for understanding the functioning of the bc_1/b_6f complexes. We were particularly interested in determining structural similarities or differences of the hemes of spinach cyt b_6f in comparison to the *R. rubrum* bc_1 complex (*36*−*38*). RR spectroscopy has been also successfully used to investigate chlorophylls and carotenoids both in isolated forms and in proteins (*39*). A second goal of this study is to characterize structural features of the Chl$_a$ and β-Car pigments bound to cyt b_6f.

MATERIALS AND METHODS

Purification of the Cytochrome b_6f Complex. The b_6f complex was prepared from spinach leaves and purified according to a six-step method based on the procedure of Hauska (*40*, *41*): (i) the chloroplast preparation was done as described (*40*); (ii) the removal of extrinsic proteins was performed with two treatments with NaBr (*10*, *41*), the pellets were resuspended and incubated for 10 min in 10 mM Tris-HCl, and 10 mM EDTA, pH 8.0, and the solutions were centrifuged for 20 min at 13000*g*; (iii) for the solubilization of cyt b_6f, the chlorophyll concentration was adjusted to 3−4 mg/mL (*10*); (iv) the cyt b_6f preparation was enriched by ammonium sulfate precipitations between 40% and 60% (*41*); (v) a sucrose density gradient (7−30%) centrifugation was performed during 18 h at 43 000 rpm; the buffer added to sucrose was 30 mM Tris−succinate, 1% cholate, 50 mM nonanoyl-*N*-methylglucamide (MEGA-9), and 0.1% soybean lecithin, pH 6.5; (vi) the "brown band" was collected on the sucrose gradient, concentrated with Centricon-50 (Amicon), and then layered onto a Bio-Gel P30 column (0.7−1.0 × 50−60 cm) equilibrated with 50 mM Tris-HCl, 0.5% cholate, and 50 mM MEGA-9, pH 8.0. The cyt b_6f fractions were pooled and concentrated with Centricon-50. The Chl$_a$/cyt *f* ratio was estimated from the amplitude of the 554 nm band in the "ascorbate-reduced" minus "oxidized" difference spectra and the intensity of the 669 nm band in the absolute spectra of the b_6f complexes. Using $\Delta\epsilon_{mM}$(554 nm) = 26 and ϵ_{mM}(669 nm) = 79 (*28*, *42*), this ratio was 1.0 ± 0.2 for the 10 preparations we investigated. The activity of cyt b_6f (1 nM), measured with 15 μM decylplastoquinol as an electron donor and 5 μM spinach plastocyanin as an electron acceptor, was 130 ± 70 electrons/s, an intermediate value among the data reported previously (*10*, *27*, *41*, *43*, *44*). The cyt b_6f complex was also checked by SDS−polyacrylamide gel electrophoresis (*10*). The cyt b_6f preparations were freshly used for absorption and RR measurements.

Four redox states of cyt b_6f were studied, i.e., the oxidized, native or "as prepared", ascorbate-reduced, and dithionite-reduced forms. The native complexes were fully oxidized with ammonium persulfate at a final concentration of 10−25 mM (*36*). The ascorbate- and dithionite-reduced b_6f complexes were prepared anaerobically with a reductant concentration of 5−30 mM (*36*).

Spectroscopy. The absorption spectra were recorded with a Cary 5E spectrometer. Resonance Raman experiments were conducted at 20 ± 1 °C using a Jobin-Yvon spectrometer (HG2S). The spectra were excited with the 441.6 nm line of a He−Cd laser (Liconix) and the 413.1 and 406.7 nm lines of a Kr^+ laser (Coherent Innova). Although the laser radiant powers we used were low (5−20 mW), heme photoreduction caused by the Soret excitations slightly increased the reduction level of one (or several) heme(s) of cyt b_6f. Cytochrome *f* was found to be particularly photoreducible even in the presence of persulfate.

The spectra were imported, checked, and analyzed with Grams/32 software (Galactic Industries). The scans of each experiment were compared and only added if no significant spectral difference was observed. The RR spectra shown are the results of unsmoothed sums (*3*−*4*) of 3−25 scans of independent preparations of cyt b_6f. To ascertain the frequency of overlapping bands, curve fittings were done with a nonlinear least-squares program of the Grams/32 software (*36*). The uncertainty range for the strongest band is 0.5−1 cm^{-1}. For the weakest bands, the frequencies are determined within 1−2 cm^{-1}.

RESULTS

Absorption Spectra. Visible absorption spectra of spinach b_6f complex are shown in Figure 1. For a given preparation, constant contributions are seen for the three absorption bands observed at 669, 483, and 435 nm in the spectra of the different redox forms. The spectra of the oxidized form exhibit a broad Soret band at 415 nm and weak features at 572 and 528 nm. Those of the native complex show a Soret band with a slightly variable position (417−419 nm) and a more or less marked α band at 554 nm (Figure 1; Table 1). Weak bands remain observable at 572 and 528 nm. The spectra of the ascorbate-reduced form show an increased intensity for the 554 nm band as well as the appearance of new bands at 533 and 524 nm. The Soret maximum is red shifted to 421 nm (Figure 1; Table 1). The difference spectra "ascorbate-reduced minus oxidized" (not shown) have three

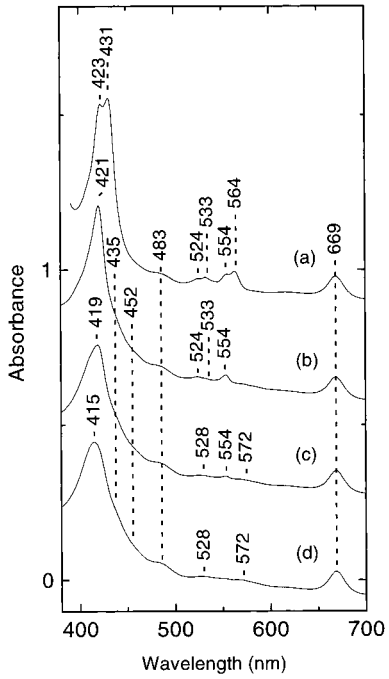

FIGURE 1: Electronic absorption spectra of spinach cyt b_6f in the dithionite-reduced (a), ascorbate-reduced (b), native (c), and persulfate-oxidized (d) forms.

Table 1: Absorption Maxima (nm) of the Spinach Cytochrome b_6f Complex

	hemes				
cyt b_6f	Soret	β	α	Chl$_a$	β-Car
oxidized	415	528	572	435, 669	452, 483
as prepared	417−419	528	554	435, 669	452, 483
ascorbate-reduced	421	524, 533	554	435, 669	452, 483
dithionite-reduced	423, 431	524, 533	554, 564	669	483

positive bands at 422, 524, and 554 nm and a negative band at 407 nm. When compared to the absorption spectrum of the ascorbate-reduced form, that of the dithionite-reduced form displays two bands at 431 and 423 nm in the Soret region and four bands at 564, 554, 533, and 524 nm in the α/β region (Figure 1). In the difference spectra "dithionite-reduced minus ascorbate-reduced", three positive bands peak at 433, 534, and 564 nm while a negative Soret contribution is observed at 413 nm (spectra not shown).

High-Frequency Regions of RR Spectra (1300−1650 cm^{-1}). Using Soret excitations, the most intense band of the RR spectra of hemes and hemoproteins is seen in the 1350−1380 cm^{-1} regions and corresponds to the redox-sensitive ν_4 mode (*36*−*38*). Figure 2 shows the 1300−1650 cm^{-1} regions of the oxidized, "as prepared", ascorbate-reduced, and dithionite-reduced forms of cyt b_6f, excited at 406.7 (Figure 2A) and 441.6 (Figure 2B) nm. The 406.7 and 413.1 nm excitations enhance ν_4 modes with bands observed at 1359−1360 and 1373−1374 cm^{-1} for the reduced and oxidized hemes, respectively (Figure 2A and spectra not shown). In the spectra of oxidized cyt b_6f, a shoulder at 1361 cm^{-1} corresponds to a slight photoreduction of the complex even in the presence of persulfate. Using the 441.6 nm excitation, the contributions of ν_4 become small in the spectra of the native and oxidized complexes (Figure 2B). The major

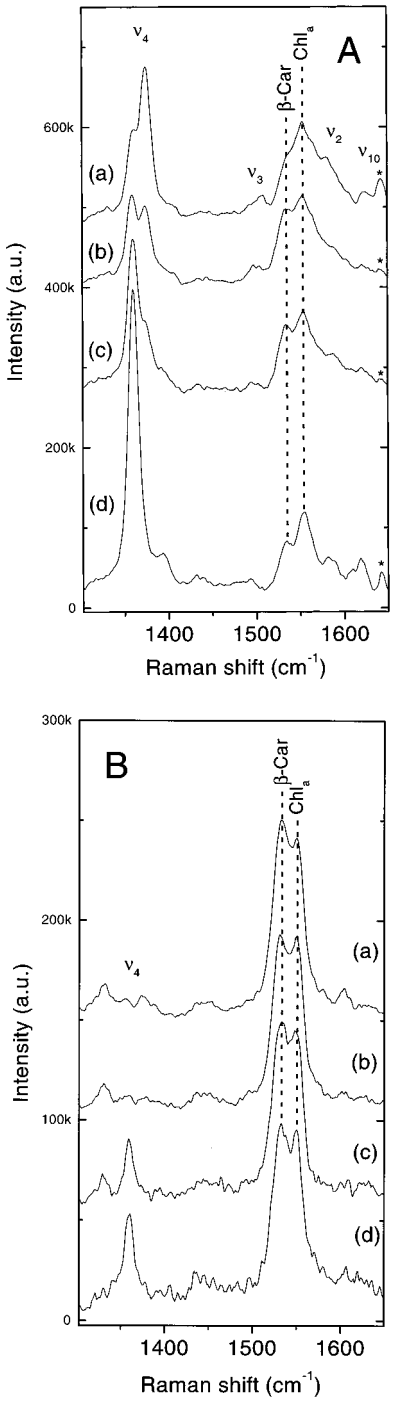

FIGURE 2: High-frequency regions (1300−1650 cm^{-1}) of RR spectra of persulfate-oxidized (a), native (b), ascorbate-reduced (c), and dithionite-reduced (d) cyt b_6f, excited at 406.7 (A) and 441.6 (B) nm (8−25 accumulated scans). In each panel, the spectra were normalized to the Chl$_a$ band at 1550−1554 cm^{-1}. In panel A, an asterisk indicates a plasma line.

spectral features are constituted by a cluster of bands in the 1520−1570 cm^{-1} regions (Figure 2B). In the RR spectra of hemes and hemoproteins, this region contains the ν_{11} (1525−1570 cm^{-1}) and ν_{38} (1550−1560 cm^{-1}) heme modes (*36*−*38*). However, Soret excitations do not permit RR enhancements of both the depolarized ν_{11} modes and the polarized ν_{38} modes with intensities largely stronger than that of the polarized ν_4 modes (*36*−*38*). Therefore, the strong bands seen in the 1520−1570 cm^{-1} regions of RR spectra of cyt b_6f cannot be assigned to heme contributions.

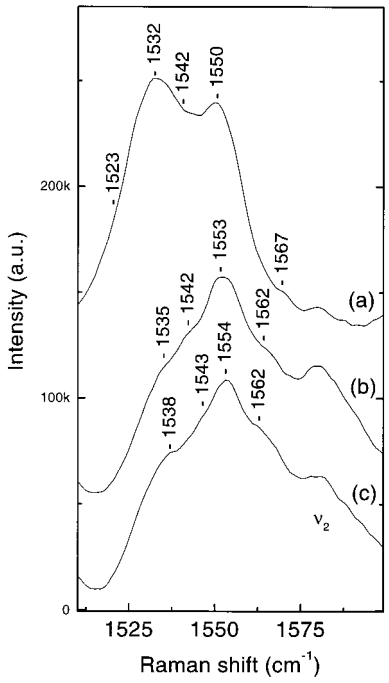

FIGURE 3: The 1510−1600 cm^{-1} regions of RR spectra of persulfate-oxidized cyt b_6f, excited at 441.6 (a), 413.1 (b), and 406.7 (c) nm (8−41 accumulated scans). The spectra were normalized to the Chl$_a$ band at ca. 1552 cm^{-1}.

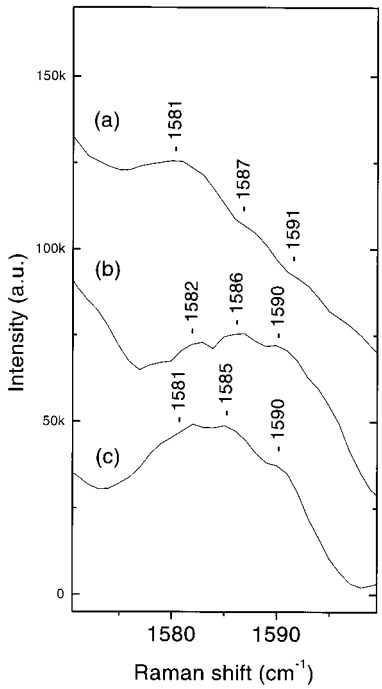

FIGURE 4: ν_2 regions (1570−1600 cm^{-1}) of RR spectra of cyt b_6f: (a) persulfate-oxidized form excited at 406.7 nm; (b) ascorbate-reduced form excited at 413.1 nm; (c) dithionite-reduced form excited at 413.1 nm (12−25 accumulated scans). The spectra were normalized to the 1552 cm^{-1} band of Chl$_a$.

(A) 1520−1570 cm^{-1} Regions. Spectral accumulations and curve fittings characterize six components in the 1520−1570 cm^{-1} regions of RR spectra of cyt b_6f. With the three excitations used, a band is detected at 1550−1554 cm^{-1} for the four redox forms. Its frequency tends to be slightly increased as the redox state of the b_6f complex is more and more reduced (spectra not shown). This apparent effect corresponds to an increased contribution of the underlying ν_{38} modes of reduced hemes. With the 441.6 nm excitation, a major band is observed at 1531 (±1) cm^{-1}. Its relative intensity is strongly decreased when the excitation is shifted to 413.1 and 406.7 nm (Figure 3 and spectra not shown). The four remaining bands have medium intensities and are detected at 1524 (±1), 1537 (±2), 1542 (±2), and 1562 (±2) cm^{-1} (Figure 3 and spectra not shown).

(B) ν_2 Regions (1570−1600 cm^{-1}). Although β-Car and Chl$_a$ largely contribute in the 1520−1570 cm^{-1} regions of RR spectra, the frequency of the ν_2 heme modes can still be determined with a sufficient precision. Spectral accumulations of the 1570−1600 cm^{-1} regions of RR spectra show three components at 1581 (±1), 1586 (±1), and 1591 (±1) cm^{-1} for the four redox states of cyt b_6f (Figure 4 and spectra not shown). Taking into account the positions of the ν_2 components on the high-frequency side of the strong 1553 and 1562 cm^{-1} bands, the relative intensities of these components depend on both the reduction level of cyt b_6f and the exciting wavelength. For the oxidized form, excited at 413.1 or 406.7 nm, the 1581 cm^{-1} component constitutes the most intense feature, and the 1591 cm^{-1} band is the least active component (Figure 4, spectrum a, and spectra not shown). The latter band becomes the most intense component in the spectra of the ascorbate-reduced form, excited at 413.1 nm (Figure 4, spectrum b). In the spectra of the dithionite-reduced form, its relative intensity is decreased to the benefit of the 1581 and 1585 cm^{-1} bands (Figure 4, spectrum c).

(C) ν_3 Regions (1490−1510 cm^{-1}). The ν_3 regions of the RR spectra of native cyt b_6f excited at 406.7 or 413.1 nm contain four overlapping bands at 1492 (±1), 1499 (±1), 1502 (±1), and 1506 (±1) cm^{-1} (spectra not shown). The cyt b_6f oxidation produces two major bands at 1506 and 1499 cm^{-1}. When the native complex is reduced by ascorbate, the contribution of the 1506 cm^{-1} band is strongly decreased while that of the 1492 cm^{-1} band increases its intensity, the intensities of the 1499 and 1502 cm^{-1} components remaining unaffected. The 1506 and 1492 cm^{-1} bands are therefore assigned to ν_3 of oxidized and reduced cyt f, respectively (Table 2). The spectra of dithionite-reduced cyt b_6f, excited at 413.1 or 406.7 nm, exhibit two bands at 1492 and 1496 cm^{-1}. Only a weak 1496 cm^{-1} band is detected in the spectra excited at 441.6 nm. The 1492 and 1496 cm^{-1} frequencies are attributed to the ν_3 modes of the reduced hemes b (Table 2).

(D) ν_{10} Regions (1610−1650 cm^{-1}). The ν_{10} bands of the ferric and ferrous hemes are well separated at 1630−1645 and 1610−1625 cm^{-1}, respectively (*36*−*38*). The 1630−1645 cm^{-1} regions of the RR spectra of oxidized and native cyt b_6f, excited at 406.7 or 413.1 nm, show three overlapping bands at 1633 (±1), 1638 (±1), and 1641 (±1) cm^{-1}. The spectra of the ascorbate-reduced complex exhibit only two of these bands at 1633 and 1641 cm^{-1} (spectra not shown). Considering that the b-type hemes of cyt b_6f remain oxidized in the presence of ascorbate, these two latter frequencies are assigned to ν_{10} modes of the oxidized b-type hemes. The 1638 cm^{-1} component is attributed to ν_{10} of oxidized cyt f (Table 2).

The 1610−1625 cm^{-1} regions of the RR spectra of oxidized and native cyt b_6f, excited at 413.1 or 406.7 nm, contain a main band at 1624 cm^{-1} with a more or less marked shoulder at 1619 cm^{-1} (spectra not shown). The reduction

Table 2: Frequency Ranges (cm^{-1}) of Heme Skeletal Modes Observed in the RR Spectra of *R. rubrum* Cyt bc_1 and Spinach Cyt b_6f

heme mode[a]	cyt bc_1 frequency (cm^{-1})	cyt b_6f frequency (cm^{-1})
ν_{10}	1639−1641 (*b*)	1640−1642 (*b*)
	1635−1639 ($b + c_1$)	1637−1638 (*f*)
		1632−1634 (*b*)
ν'_{10}	1617−1618 (c_1)	1618−1620 (*f*)
	1614 (b_H)	1617−1619 (*b*)
	1610−1611 (b_L)	1608−1610 (*b*)
ν_2, ν'_2	1578−1581 (b_L)	1579−1582 (*b*)
	1582−1585 (b_H)	1585−1587 (*b*)
	1587−1590 (c_1)	1590−1592 (*f*)
ν_3	1500−1505 ($b + c_1$)	1505−1506 (*f*)
		1501−1503 (*b*)
		1499−1500 (*b*)
ν'_3	1491−1495 ($b + c_1$)	1495−1496 (*b*)
		1491−1492 (*f*)
		1492 (*b*)
ν_4	1371−1374 ($b + c_1$)	1372−1374 ($b + f$)
ν'_4	1359−1363 ($b + c_1$)	1359−1363 ($b + f$)
ν_8, ν'_8	351−353 (b_L)	355−357 (*f*)
	346−349 (c_1)	350−352 (*b*)
	344−345 (b_H)	345−346 (*b*)

[a] ν_x and ν'_x correspond to assignments for oxidized and reduced heme species, respectively. The RR data on cyt bc_1 are from ref *36*.

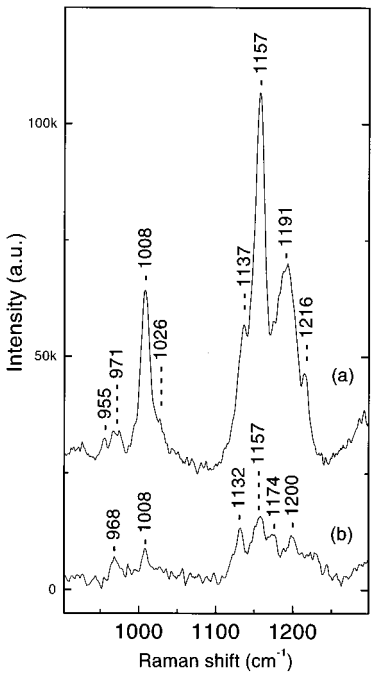

FIGURE 5: Medium-frequency regions (900−1300 cm^{-1}) of RR spectra of oxidized cyt b_6f excited at 441.6 (a) and 406.7 (b) nm (3−7 accumulated scans).

of cyt b_6f by ascorbate increases the intensity of the 1619 cm^{-1} band relative to that of the 1624 cm^{-1} band. The 1619 cm^{-1} band is therefore assigned to ν_{10} of reduced cyt *f* (Table 2) while the 1624 cm^{-1} band likely corresponds to a stretching mode of the vinyl groups of the *b*-type hemes (*36*, *38*). The full reduction of cyt b_6f produces a large increase in intensity of two bands at 1618 and 1610 cm^{-1}. These bands are assigned to the ν_{10} modes of the reduced *b*-type hemes (Table 2). Shoulders observed at 1623 and 1626 cm^{-1} are attributable to vinyl stretching modes of the reduced *b*-type hemes.

Mid-Frequency Regions of RR Spectra (900−1300 cm^{-1}). The RR spectra of cyt b_6f exhibit strong bands in the 900−1300 cm^{-1} regions. In particular, the spectra of the native and oxidized forms, excited at 441.6 nm, show these bands at 1008 (±1), 1137 (±2), 1157 (±1), 1191 (±1), and 1216 (±2) cm^{-1} (Figure 5, spectrum a, and data not shown). These bands are either weak or absent in the spectra excited at 406.7 nm (Figure 5, spectrum b).

Low-Frequency Regions of RR spectra (150−450 cm^{-1}). The RR spectra of cyt b_6f excited at 441.6, 413.1, or 406.7 nm exhibit a number of low-frequency bands. Figure 6A displays the spectra of oxidized, ascorbate-reduced, and dithionite-reduced cyt b_6f, excited at 413.1 nm. In these spectra as well as in those excited at 406.7 or 441.6 nm, there is no apparent RR contribution arising from either Chl_a or β-Car. The most intense bands in the RR spectra are broad and are observed in the 340−360 cm^{-1} regions (Figure 6A). They were assigned to ν_8 modes that are sensitive to the heme structure (*36*−*38*).

The RR spectra of oxidized cyt b_6f excited at 406.7 or 413.1 nm exhibit an asymmetric ν_8 band (Figure 6A and spectra not shown). Large accumulations of the RR data in fact show that it contains a main component at 356 (± 1) cm^{-1} and two marked shoulders at 345 (± 1) and 351 (± 1) cm^{-1} (Figure 6B, spectrum a, and spectra not shown). When the excitation is blue shifted to 441.6 nm, a very weak ν_8 band is centered at 352 cm^{-1} (spectrum not shown). The RR spectra of the native and ascorbate-reduced complexes, excited at 413.1 or 406.7 nm, are very close and produce a major band at 357 cm^{-1} (Figure 6B, spectrum b, and spectra not shown). Weaker ν_8 components are, however, detected at 345 and 350−351 cm^{-1}. The RR spectra of dithionite-reduced cyt b_6f excited at 406.7 or 413.1 nm maintain a major ν_8 band at 357 cm^{-1} (Figure 6B, spectrum c, and spectra not shown). However, the components at 345−346 and 351−352 cm^{-1} increase in relative intensity when the spectra are compared to those of the ascorbate-reduced form (Figure 6B, spectra b and c). Using the 441.6 nm excitation, the contribution of the 357 cm^{-1} band is decreased while the relative intensities of the 345 and 351 cm^{-1} components are significantly increased (Figure 6B, spectra c and d). The shoulders observed at 361−364 cm^{-1} are assigned to a ν_{50} mode of oxidized or reduced cyt *f*. Weak bands detected at 337−341 cm^{-1} correspond to γ_6 heme modes (*36*−*38*).

DISCUSSION

Redox Titrations and Absorption Properties of the Chromophores of the Cytochrome b_6f Complex. The redox potentials of the *f*-, b_H-, and b_L-hemes of spinach cyt b_6f complex at pH 7.4 are +339, −60, and −188 mV, respectively (*21*). The midpoint potentials of hemes b_H and b_L are respectively decreased to −112 and −215 mV at pH 8.3. The redox potential of cyt *f* is pH independent between 6.5 and 8.3 (*21*).

The absorption spectra of persulfate-treated cyt b_6f show that the three hemes are fully oxidized (Table 1). With an E_{m8} value of +30 mV (*45*), ascorbate reduces cyt *f* but not the two *b*-type hemes of cyt b_6. Considering the absolute and difference spectra of oxidized and ascorbate-reduced cyt b_6f, the absorption bands observed at 422, 524, and 554 nm are clearly characteristic of ferrous cyt *f* (*46*). The negative band seen at 407 nm in the ascorbate-reduced minus oxidized

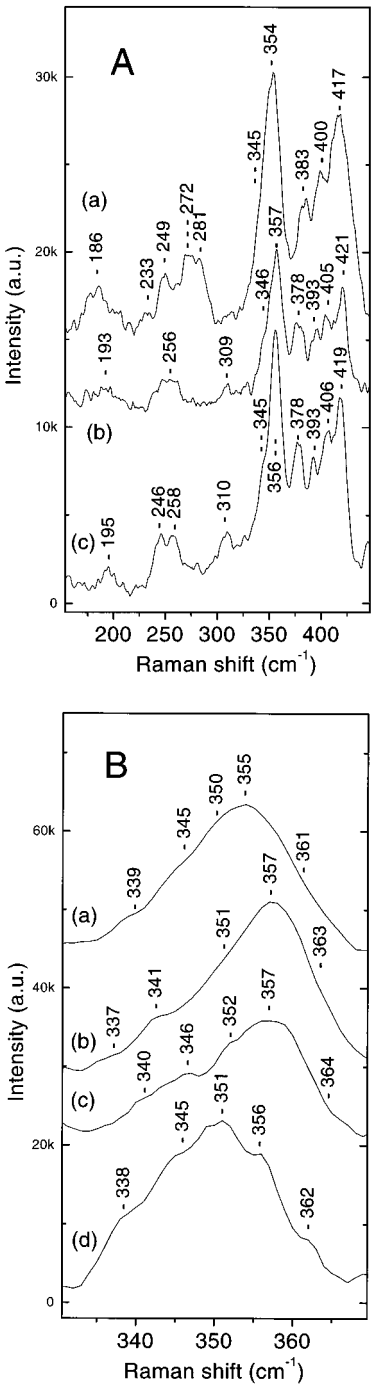

FIGURE 6: (A) Low-frequency regions (150−450 cm^{-1}) of RR spectra of persulfate-oxidized (a), ascorbate-reduced (b), and dithionite-reduced (c) cyt b_6f, excited at 413.1 nm (5−8 accumulated scans). (B) ν_8 regions (330−370 cm^{-1}) of RR spectra of cyt b_6f in the persulfate-oxidized form, excited at 413.1 nm (a), the ascorbate-reduced form, excited at 413.1 nm (b), and the dithionite-reduced form, excited at 413.1 (c) and 441.6 (d) nm (23−72 accumulated scans).

difference spectra is associated with the Soret contribution of ferric cyt *f*. On the basis of the presence of an absorption band at 554 nm (Table 1), one can conclude that native cyt b_6f has its cyt *f* partially reduced while the hemes of cyt b_6 are fully oxidized. Dithionite ($E_{m8} = -780$ mV) (*47*) fully reduces the three hemes of cyt b_6f. The contributions of the ferrous *b*-type hemes are detected at 433, 534, and 564 nm in the dithionite-reduced minus ascorbate-reduced difference spectra. The negative band detected at 413 nm in the dithionite-reduced minus ascorbate-reduced spectra is assigned to the Soret contribution of the oxidized *b*-type hemes.

The bands seen at 669 and 435 nm in the spectra of the different redox states of cyt b_6f are associated with Chl$_a$ specifically bound to cyt b_6f (*2*, *26*, *27*, *48*). The weak features observed at 452 and 483 nm are correlated with b_6f-bound β-Car (*26*, *27*, *48*).

RR Spectroscopy of the Pigments Bound to Cytochrome b_6f. The present investigation reports the RR spectra of the spinach cyt b_6f complex, excited at 441.6, 413.1, and 406.7 nm. These wavelengths were selected to excite different RR contributions of the chromophores included in the b_6f complex. A number of strong bands are observed in the RR spectra of cyt b_6f but not in those of the cyt bc_1 complexes (*36*). Table 3 lists the frequencies of the additional bands assignable to vibrational modes of either Chl$_a$ or β-Car. The 441.6 nm excitation of oxidized and native cyt b_6f is expected to strongly enhance RR modes of Chl$_a$ and β-Car since it falls close to an electronic transition of these pigments, i.e., the B_x transition of Chl$_a$ (430−445 nm) and the $A_g^- \rightarrow B_u^+$ (1-0) transition of β-Car (445−450 nm) (*39*, *49*−*51*). This excitation is also relatively far from the Soret transitions of the oxidized hemes (407 and 413 nm). The most intense bands in the high-frequency RR spectra of cyt b_6f excited at 441.6 nm are observed in the 1520−1575 cm^{-1} frequency range. Previously published data show that this region contains strong RR bands of chlorophylls and carotenoids (*39*). With the 413.1 and 406.7 nm excitations, Chl$_a$ modes remain observable due to a resonance effect on the B_y transition (410−420 nm). On the contrary, shifting the excitation from 441.6 to 413.1 and 406.7 nm decreases the relative contribution of the β-Car modes, the two violet excitations being well away from the $A_g^- \rightarrow B_u^+$ transitions (452 and 483 nm).

(A) Chlorophyll a. Table 3 shows the frequencies of the RR bands assignable to Chl$_a$ bound to cyt b_6f. The width of the RR bands (12−14 cm^{-1}) indicates a homogeneous structure and environment for the bound Chl$_a$ molecules. The phorbin modes at 1606, 1552, and 1524 cm^{-1} (Table 3) are clearly indicative of a five-coordinated Mg atom (*52*). Homologous frequencies at 1610, 1556, and 1527 cm^{-1} were characterized in the line-narrowed emission spectra of Chl$_a$ bound to a monomeric b_6f complex (*48*). These frequencies are also in agreement with a single axial ligand for Chl$_a$. However, the 3−4 cm^{-1} shifts indicate a change in the Chl$_a$ environment between the two cyt b_6f complexes. Chl$_a$ was located in the cyt b_6 subunit (*29*). The interface of the cyt b_6f dimer is constituted by cyt b_6, subunit IV, and the Rieske protein, the latter protein being absent in the monomeric complex (*8*, *48*). The frequency shifts observed for the phorbin modes thus suggest that the Chl$_a$ site is close to the dimerization interface involving cyt b_6. The role of Chl$_a$ is unclear but is presumably structural in stabilizing a dimeric state for the cyt b_6f complex.

(B) β-Carotene. β-Carotene is bound to various b_6f complexes (*27*, *28*). After extraction, purification, and dissolution in *n*-hexane, the absorption spectrum of the carotenoid isolated from cyt b_6f resembles that of 9-*cis* or 15-*cis* β-Car (*28*). The 441.6 nm excitation of spinach cyt b_6f enhances strong contributions of β-Car at 1531, 1191, 1157, and 1008 cm^{-1} (Table 3). A normal-coordinate analysis

Table 3: Frequencies of the Observed RR Modes of Chlorophyll *a* and β-Carotene Bound to the Spinach Cytochrome b_6f Complex

frequency (cm^{-1})	mode assignment[a,b]	frequency (cm^{-1})	mode assignment[a,b]
1606	Chl_a [$\nu(C_aC_m)$]	1322	β-Car [$\delta(C_{12}-H)$, $\nu(C_{11}=C_{12})$]
1552	Chl_a [$\nu(C_aC_b)$, $\nu(C_bC_b)$]	1216	β-Car [$\nu(C_{12}-C_{13})$, $\delta(C_{14}-H)$]
1542	Chl_a [$\nu(C_bC_b)$]	1200	Chl_a [$\gamma(C_bH)$]
1531	β-Car [$\nu(C_{13}=C_{14})$, $\nu(C_{11}=C_{12})$]	1191	β-Car [$\delta(C_{10}-H)$, $\delta(C_{11}-H)$]
1524	Chl_a [$\nu(C_bC_b)$, $\nu(C_aC_b)$]	1186	Chl_a [$\nu(C_mC_{10})$, δ (C_bH)]
1495	Chl_a [$\nu(C_aC_m)$, $\nu(C_aC_b)$]	1157	β-Car [$\nu(C_{14}-C_{15})$, $\delta(C_{15}-H)$]
1450	β-Car [δ_{as}(9Me), δ_{as}(13Me)]	1145	Chl_a [$\nu(C_aN)$, $\delta(C_aNC_a)$]
1442	Chl_a [ν(CC)]	1137	β-Car [$\nu(C_{10}-C_{11})$]
1437	Chl_a [$\nu(C_aC_m)$, $\nu(C_aC_b)$]	1026	β-Car [ρ(9Me), $\nu(C_8-C_9)$]
1389	β-Car [δ_s(9Me), δ_s(13Me)]	1008	β-Car [ρ(13Me), $\nu(C_{12}-C_{13})$]
1356	Chl_a [$\nu(C_aN)$]	971	β-Car [$\tau(C_{11}=C_{12})$]
1330	Chl_a [$\nu(C_aN)$, $\delta(C_mH)$]	968	Chl_a [$\delta(C_mC_aN)$, $\nu(C_9C_{10})$]

[a] Assignment for Chl_a from ref *39*. [b] Assignment for β-Car from ref *53*.

assigned the strong band at 1530−1540 cm^{-1} to an in-phase C=C stretching mode (ν_1) (*53*). Moreover, the frequency of this mode easily distinguishes stretched or terminal-bent configurations from central-bent configurations. For β-Car dissolved in cyclohexane or CS_2, the *all-trans*, 7-*cis*, and 11-*cis* configurations exhibit ν_1 at 1529−1530 cm^{-1} while this frequency is shifted to 1534 cm^{-1} for the 9-*cis* isomer and to 1539−1540 cm^{-1} for the 13-*cis* and 15-*cis* isomers (*53*). On the basis of a ν_1 frequency at 1531 cm^{-1} (Table 3), the conformation of the β-Car bound to cyt b_6f is therefore *all-trans*, 7-*cis*, or 11-*cis*. In the mid-frequency regions, structure-sensitive bands were detected at 1274 cm^{-1} for the 7-*cis* form and at 1268 cm^{-1} for the 11-*cis* form (*51*). Since these bands are absent in the spectra of β-Car bound to cyt b_6f, the *all-trans* configuration is the most probable. The relative intensities of the bands at ca. 1160, 1140, and 1006 cm^{-1} are sensitive to the configuration of β-Car (*51*). The spectral features observed in Figure 5 are also in agreement with an *all-trans* configuration for the bound β-Car.

It is difficult to rationalize a correlation between the carotenoid function and the polyene conformation. However, the carotenoids involved in photosynthetic complexes are either *all-trans* or 15-*cis* (*39*, *51*). *All-trans* forms were related with a good efficiency for energy transfer in antenna proteins, and 15-*cis* forms were associated with a photoprotective function in reaction centers (*51*). It was proposed that β-Car bound to cyt b_6f prevents generation of singlet O_2 from the photoexcited Chl_a (*28*). Our RR data indicate that β-Car can fulfill this scavenging role in adopting an *all-trans* configuration.

Assignment of the Heme Modes. To assign the RR bands in terms of individual heme groups, we have exploited the different optical and redox properties of the *b*- and *c*-type hemes (*36*). On one hand, the Soret band has its position considerably red shifted and its intensity increased when a *b*- or *c*-type heme is reduced (*36*). On the other hand, the different peripheral compositions of the *b*- and *c*-type hemes affect the Soret band position as well as the RR frequency of some porphyrin modes (*36*). These cumulated effects produced differential enhancements for a number of RR bands of the three hemes of cyt bc_1 (*36*). Given the similarities in heme compositions and absorption properties of the bc_1/b_6f complexes, differential RR enhancements are also expected for the hemes of cyt b_6f. In relation to the redox states of the b_6f complex and the excitations used, a careful analysis of the frequency and/or intensity dependence(s) of the RR bands allowed us to assign spectral contributions to the *b*- and *c*-type hemes.

Heme Structures in the Spinach Cytochrome b_6f Complex. The RR spectra of spinach cyt b_6f show three components for the ν_2, ν_3, ν_8, and ν_{10} modes (Table 2). This observation is similar to that made from RR spectra of *R. rubrum* cyt bc_1 and indicates different structures for the three hemes of cyt b_6f (*36*).

(A) The c-Type Heme of Cytochrome f. The selective reduction of cyt *f* by ascorbate permits the characterization of RR modes of oxidized and reduced cyt *f*. In this way, ν_3 and ν_{10} are respectively assigned at 1506 and 1638 cm^{-1} for oxidized cyt *f* and at 1492 and 1619 cm^{-1} for reduced cyt *f* (Table 2). The frequencies of ν_2 and ν_8 are weakly sensitive to the oxidation state of the heme (*36*). Therefore, the reduction of cyt *f* is expected to essentially modify the intensity of these modes. In the spectra of the ascorbate-reduced form excited at 413.1 nm, the major intensity observed for the 1591 cm^{-1} component favors an assignment to the ν_2 mode of cyt *f*. The elevated ν_2 frequencies observed for the *c*-type hemes over the *b*-type hemes (*36*−*38*) also support this assignment (Table 2). The assignment of the 355−357 cm^{-1} band to ν_8 of cyt *f* is essentially based on the decreases in relative band intensity provoked by either the reduction of the *b*-type hemes or the red shift of the excitation from 413.1 to 441.6 nm.

The soluble domain of turnip cyt *f* was crystallized and its atomic structure solved (*30*). The axial heme ligands are the His residue of the -C-x-y-C-H- characteristic sequence of the *c*-type hemes and the α-amino group of the N-terminal residue (*31*). In the RR spectra of this truncated ferrous cyt *f*, the ν_{10}, ν_2, ν_3, and ν_8 modes were respectively characterized at 1618, 1589, 1491, and 356 cm^{-1} (*54*−*57*). All of these frequencies are in agreement with a His/amine coordination (*58*). One may argue that the exceptional His/amine coordination found for the soluble part of cyt *f* could be an artifact of protein preparation. The very close RR data obtained for the skeletal modes of isolated and b_6f-bound cyt *f* demonstrate that the His/amine coordination is specific to the full cyt *f*, inserted in the complex. Several low-frequency bands assigned to modes of the heme substituents (417, 306, and 199 cm^{-1} for isolated cyt *f* versus 421, 309, and 193 cm^{-1} for bound cyt *f*) exhibit frequency differences that can be interpreted in terms of slight changes in peripheral heme−protein interactions.

(B) The b-Type Hemes of Cytochrome b_6. Due to their low potentials, the *b*-type hemes of cyt b_6f are fully oxidized in the oxidized, native, and ascorbate-reduced forms and fully reduced in the dithionite-reduced form. Band splittings are found in the RR spectra of the various redox states of cyt b_6f, but we cannot assign the vibrational components to either heme b_H or heme b_L. This situation differs from that encountered for *R. rubrum* cyt bc_1 for which heme b_H is partially reduced by ascorbate (*36*).

The ν_2 modes of the *b*-type hemes are assigned at 1581 and 1586 cm^{-1} (Table 2). These assignments can be made by exclusion of the 1591 cm^{-1} band attributed to the ν_2 mode of cyt *f*. Nevertheless, internal consistencies due to differential resonance effects allow a confirmation of these assignments. For example, in the RR spectra of oxidized cyt b_6f excited at 413.1 nm, the 1581 and 1586 cm^{-1} components are the most active. This effect is due to a laser excitation closer to the Soret enveloppe of the oxidized *b*-type hemes (413 nm) than that of oxidized cyt *f* (407 nm). Similarly, the 345 and 351 cm^{-1} bands are assigned to the ν_8 modes of the *b*-type hemes. In the RR spectra of the dithionite-reduced form, the relative intensity of these bands is increased when the excitation is changed from 413.1 to 441.6 nm. This increase in relative enhancement is interpreted in the context of a better resonance for the ν_8 modes of the reduced *b*-type hemes (Soret band at 433 nm) than for the ν_8 mode of reduced cyt *f* (Soret band at 422 nm).

The RR spectra of the bc_1 complex showed different contributions for the ν_2, ν_8, and ν_{10} modes (*36*). Frequencies at 1580 (ν_2), 352 (ν_8), and 1610 (ν_{10}) cm^{-1} were assigned to the b_L-heme of cyt bc_1. On the basis of comparisons with data obtained for model compounds, these frequencies were interpreted in the frame of a strongly distorted macrocycle. A very close set of frequencies (1581, 351, and 1610 cm^{-1}) is detected in the RR spectra of spinach cyt b_6f (Table 2) and indicates a similar distortion for one of the *b*-type hemes of cyt b_6f.

The ν_2, ν_8, and ν_{10} frequencies of the reduced b_H-heme of cyt bc_1 were respectively characterized at 1584, 344, and 1614 cm^{-1} and associated with a slightly distorted structure for heme b_H of cyt bc_1 (*36*). In the RR spectra of cyt b_6f, homologous bands are observed at 1586, 345, and 1618 cm^{-1} (Table 2). These small upshifts of the ν_2 (+2 cm^{-1}), ν_8 (+1 cm^{-1}), and ν_{10} (+4 cm^{-1}) modes likely reflect a planar conformation for the corresponding *b*-type heme in cyt b_6f (*36*).

From the results of this investigation, it could be tempting to conclude that heme b_L of *R. rubrum* cyt bc_1 and of spinach cyt b_6f has a conserved distorted structure while heme b_H adopts either a slight distorted structure in cyt bc_1 or a planar structure in cyt b_6f. This small difference in the conformation of the b_H-hemes could be correlated with the positions of the His ligands of the b_H- and b_L-hemes. Using the sequence homologies with the bovine bc_1 complex, the His ligands in helix D of *R. rubrum* cyt bc_1 (His-195 and -209) and of spinach cyt b_6f (His-187 and -202) are respectively spaced by 13 and 14 amino acid residues (*59*, *60*). The additional residue in cyt b_6 could induce a release in protein constraint allowing the b_H-heme to be more planar in cyt b_6 than in cyt *b*.

Since this RR investigation does not discriminate between the *b*-type hemes of spinach cyt b_6f, we cannot dismiss the alternative view considering heme b_H more distorted than heme b_L. This situation is observed in the X-ray structures of mitochondrial bc_1 complexes (*7*, *30*). An inspection of the structures of the chicken complex in the presence or absence of Q_o (and Q_i) inhibitor(s), however, reveals that the binding of the Q_o site produces a strong decrease in the out-of-plane deformation of heme b_H (*30*, *61*). Recalling that the RR data obtained on *R. rubrum* cyt bc_1 suggest that heme b_L is more distorted than heme b_H (*36*), the different heme conformations observed between the mitochondrial and bacterial complexes would be related to different orientations of the b_L- and b_H-hemes, likely induced by the different oligomerization states of the bc_1/b_6f complexes (*62*, *63*).

The different conformations of hemes b_H and b_L of *R. rubrum* cyt bc_1 were in part related to their different midpoint potentials (*36*). Considering the plausible role of the porphyrin deformations on the hemoprotein functions (*64*), further RR studies are presently necessary to determine the influence of the protein−protein and protein−cofactor interactions, i.e., the number of proteins forming the complex, the conformation of the Rieske protein, and the occupation of the Q_o and Q_i sites, on the structures of the *b*-type hemes of the bc_1/b_6f complexes.

CONCLUSION

The Soret-excited RR spectra of spinach cyt b_6f contain vibrational contributions from Chl_a, β-Car, and the hemes of cyt *f* and cyt b_6. In the absence of crystal structures, several useful conclusions can be drawn from the results of this investigation: (i) the identified phorbin modes clearly indicate that Chl_a has one axial ligand and is confined in a site likely close to the monomer−monomer interface; (ii) the vibrational pattern of the bound β-Car shows that it can perform its protective function in the *all-trans* configuration; (iii) the RR data demonstrate that the His/amine ligation previously characterized for truncated cyt *f* is specific of the cyt *f* included in the b_6f complex; (iv) finally, our study shows a strongly distorted conformation and a planar conformation for the two *b*-type hemes of cyt b_6f. This structural difference appears to be a common structural feature for the bc_1/b_6f complexes.

REFERENCES

1. Hauska, G., Schütz, M., and Büttner, M. (1996) in *Oxygenic Photosynthesis: The Light Reactions* (Ort, D. R., and Yocum, C. F., Eds.) pp 377−398, Kluwer Academic Publishers, Dordrecht, The Netherlands.
2. Cramer, W. A., Soriano, G. M., Ponomarev, M., Huang, D., Zhang, H., Martinez, S. E., and Smith, J. L. (1996) *Annu. Rev. Plant Physiol. Plant Mol. Biol. 47*, 477−508.
3. Cramer, W. A., Martinez, S. E., Furbacher, P. N., Huang, D., and Smith, J. L. (1994) *Cur. Opin. Struct. Biol. 4*, 536−544.
4. Gennis, R. B., Barquera, B., Hacker, B., Van Doren, S. R., Arnaud, S., Croft, A. R., Davidson, E., Gray, K. A., and Daldal, F. (1993) *J. Bioenerg. Biomembr. 25*, 195−209.
5. Brandt, U., and Trumpower, B. (1994) *Crit. Rev. Biochem. Mol. Biol. 29*, 165−197.
6. Widger, W. R., Cramer, W. A., Herrmann, R. G., and Trebst, A. (1984) *Proc. Natl. Acad. Sci. U.S.A. 81*, 674−678.
7. Xia, D., Yu, C.-A., Kim, H., Xia, J.-Z., Kachurin, A. M., Zhang, L., Yu, L., and Deisenhofer, J. (1997) *Science 277*, 60−67.
8. Mosser, G., Breyton, C., Olofsson, A., Popot, J.-L., and Rigaud, J.-L. (1997) *J. Biol. Chem. 272*, 20263−20268.

9. Iwata, S., Lee, J. W., Okada, K., Lee, J. K., Iwata, M., Rasmussen, B., Link, T. A., Ramaswamy, S., and Jap, B. K. (1998) *Science 281*, 64−71.
10. Huang, D., Everly, R. M., Cheng, R. H., Heymann, J. B., Schägger, H., Sled, V., Ohnishi, T., Baker, T. S., and Cramer, W. A. (1994) *Biochemistry 33*, 4401−4409.
11. Breyton, C., Tribet, C., Olive, J., Dubacq, J.-P., and Popot, J.-L. (1997) *J. Biol. Chem. 272*, 21892−21900.
12. Cramer, W. A., Martinez, S. E., Huang, D., Tae, G.-S., Everly, R. M., Heymann, J. B., Cheng, R. H., Baker, T. S., and Smith, J. L. (1994) *J. Bioenerg. Biomembr. 26*, 31−47.
13. Pierre, Y., Breyton, C., Kramer, D., and Popot, J.-L. (1995) *J. Biol. Chem. 270*, 29342−29349.
14. Kramer, D. M., and Croft, A. R. (1994) *Biochim. Biophys. Acta 1184*, 193−201.
15. Hauska, G., Nitschke, W., and Herrmann, R. G. (1994) *J. Bioenerg. Biomembr. 20*, 211−228.
16. Degli Esposti, M., De Vries, S., Crimi, M., Ghelli, A., Patarnello, T., and Meyer, A. (1993) *Biochim. Biophys. Acta 1143*, 243−271.
17. Hauska, G., Hurt, E., Gabellini, N., and Lockau, W. (1983) *Biochim. Biophys. Acta 726*, 97−133.
18. Nitschke, W., Hauska, G., and Croft, A. R. (1988) *FEBS Lett. 232*, 204−208.
19. Salerno, J. C. (1984) *J. Biol. Chem. 259*, 2331−2336.
20. Nitschke, W., and Hauska, G. (1987) *FEBS Lett. 213*, 453−455.
21. Hurt, E. C., and Hauska, G. (1982) *J. Bioenerg. Biomembr. 14*, 405−424.
22. Hauska, G., Hurt, E., Gabellini, N., and Lockau, W. (1983) *Biochim. Biophys. Acta 726*, 97−133.
23. Ponamarev, M. V., Schlarb, B. G., Howe, C. J., Carrell, C. J., Smith, J. L., Bendall, D. S., and Cramer, W. A. (2000) *Biochemistry 39*, 5971−5976.
24. Malkin, R. (1986) *FEBS Lett. 208*, 317−320.
25. Zhang, H., Carell, C. J., Huang, D., Sled, V., Ohnishi, T., Smith, J. L., and Cramer, W. A. (1996) *J. Biol. Chem. 271*, 31360−31366.
26. Bald, D., Kruip, E., Boekema, E. J., and Rögner, M. (1992) in *Photosynthesis: From Light to Biosphere* (Murata, N., Ed.) Part I, pp 629−633, Kluwer Academic Publishers, Dordrecht, The Netherlands.
27. Pierre, Y., Breyton, C., Lemoine, Y., Robert, B., Vernotte, C., and Popot, J.-L. (1997) *J. Biol. Chem. 272*, 21901−21908.
28. Zhang, H., Huang, D., and Cramer, W. A. (1999) *J. Biol. Chem. 274*, 1581−1587.
29. Poggese, C., Polverino de Laureto, P., Giacometti, G. M., Rigoni, F., and Barbato, R. (1997) *FEBS Lett. 414*, 585−589.
30. Zhang, Z., Huang, L., Shulmeister, V. M., Chi, Y.-I., Kim, K. K., Hung, L.-W., Croft, A., Berry, E. A., and Kim, S.-H. (1998) *Nature 392*, 677−684.
31. Martinez, S. E., Huang, D., Ponomarev, M., Cramer, W. A., and Smith, J. L. (1996) *Protein Sci. 5*, 1081−1092.
32. Iwata, S., Saynovits, M., Link, T. A., and Michel, H. (1996) *Structure 4*, 567−579.
33. Carrell, C. J., Zhang, H., Cramer, W. A., and Smith, J. L. (1997) *Structure 5*, 1613−1625.
34. Carrell, C. J., Schlarb, B. G., Bendall, D. S., Howe, C. J., Cramer, W. A., and Smith, J. L. (1999) *Biochemistry 38*, 9590−9599.
35. Chi, Y.-I., Huang, L.-S., Zhang, Z., Fernandez-Velasco, J. G., and Berry, E. A. (2000) *Biochemistry 39*, 7689−7701.
36. Le Moigne, C., Schoepp, B., Othman, S., Verméglio, A., and Desbois, A. (1999) *Biochemistry 38*, 1066−1076.
37. Hu, S., Morris, I. K., Singh, J. P., Smith, K. M., and Spiro, T. G. (1993) *J. Am. Chem. Soc. 115*, 12446−12458.
38. Hu, S., Smith, K. M., and Spiro, T. G. (1996) *J. Am. Chem. Soc. 118*, 12638−12646.
39. Lutz, M. (1984) in *Advances in Infrared and Raman Spectroscopy* (Clark, R. J. H., and Hester, R. E., Eds.) Vol. 11, pp 211−300, J. Wiley and Sons, Chichester.
40. Hurt, E. C., and Hauska, G. (1981) *Eur. J. Biochem. 117*, 591−599.
41. Hauska, G. (1986) *Methods Enzymol. 126*, 271−285.
42. Metzger, S. U., Cramer, W. A., and Whitmarsh, J. (1997) *Biochim. Biophys. Acta 1319*, 233−241.
43. Black, M. T., Widger, W. R., and Cramer, W. A. (1987) *Arch. Biochem. Biophys. 252*, 655−661.
44. Dietrich, J., and Kühlbrandt, W. (1999) *FEBS Lett. 463*, 97−102.
45. Creutz, C. (1981) *Inorg. Chem. 20*, 4449−4452.
46. Ho, K. K., and Krogman, D. W. (1980) *J. Biol. Chem. 255*, 3855−3861.
47. Mayhew, S. G. (1978) *Eur. J. Biochem. 85*, 535−547.
48. Peterman, E. J. G., Wenk, S.-O., Pullerits, T., Palsson, L.-O., van Grondelle, R., Dekker, J. P., Rögner, M., and Van Amerongen, H. (1998) *Biophys. J. 75*, 389−398.
49. Lutz, M., and Robert, B. (1988) in *Biological Applications of Raman Spectroscopy* (Spiro, T. G., Ed.) Vol. 3, pp 347−411, J. Wiley and Sons, New York.
50. Thomas, L. L., Kim, J. H., and Cotton, T. M. (1990) *J. Am. Chem. Soc. 112*, 9378−9386.
51. Koyama, Y., and Fujii, R. (1999) in *The Photochemistry of Carotenoids* (Frank, H. A., Young, A. J., Britton, G., and Cogdell, R. J., Eds.) pp 161−188, Kluwer Academic Publishers, Dordrecht, The Netherlands.
52. Fujiwara, M., and Tasumi, M. (1986) *J. Phys. Chem. 90*, 250−255.
53. Saito, S., and Tasumi, M. (1983) *J. Raman Spectrosc. 14*, 310−321.
54. Desbois, A., and Lutz, M. (1984) in *Proceedings of the IXth International Conference on Raman Spectroscopy*, pp 480−481, The Chemical Society of Japan, Tokyo.
55. Davis, D. J., Frame, M. K., and Johnson, D. A. (1988) *Biochim. Biophys. Acta 936*, 61−66.
56. Hobbs, J. D., Wynn, M., Nunez, D. J., Malkin, R., Knaff, D. B., and Ondrias, M. R. (1991) *Biochim. Biophys. Acta 1059*, 37−44.
57. Desbois, A. (1994) *Biochimie 76*, 693−707.
58. Othman, S., and Desbois, A. (1998) *Eur. Biophys. J. 28*, 12−25.
59. Heinemeyer, W., Alt, J., and Herrmann, R. G. (1984) *Curr. Genet. 8*, 543−549.
60. Majewski, C., and Trebst, A. (1990) *Mol. Gen. Genet. 224*, 373−382.
61. Crofts, A. R., Hong, S., Ugulava, N., Barquera, B., Gennis, R., Guergova-Kuras, M., and Berry, E. A. (1999) *Proc. Natl. Acad. Sci. U.S.A. 96*, 10021−10026.
62. Schoepp, B., Breton, J., Parot, P., and Verméglio, A. (2000) *J. Biol. Chem. 275*, 5284−5290.
63. Schoepp, B., Chabaud, E., Breyton, C., Verméglio, A., and Popot, J.-L. (2000) *J. Biol. Chem. 275*, 5275−5283.
64. Shelnutt, J. A., Song, X.-Z., Ma, J.-G., Jia, S.-L., Jentzen, W., and Medforth, C. J. (1998) *Chem. Soc. Rev. 27*, 31−41.

BI0106641